Electronic Supplementary Information

Unveiling the unprecedented catalytic capability of micro-sized Co-ZIF-L for the thermal decomposition of RDX by 2D-structure-induced mechanism reversal

Jia-Tong Ren, Ding Wei, Bo-Jun Tan,* Rui Hu, Yu-Chen Gao, Xiao-Hong Wang and Wei-Tao Yang*

Xi'an Modern Chemistry Research Institute, Xi'an, Shaanxi, 710065, China. E-mail: renjtongpku@163.com, tanbj204@163.com, njyangweitao@163.com

Experimental section

Caution

Cyclotrimethylenetrinitramine (RDX) is an energetic material which is sensitive towards impact and friction. Necessary safeguard procedures must be adopted when handling it or mixtures containing it, including safety glasses, face shield, latex gloves, body armor and grounded equipments.

Chemicals

The employed reagents and solvents, including $Co(NO_3)_2 \cdot 6H_2O$ (A.R.), 2-methylimidazole (2-MI, A.R.), anhydrous methanol (CH_3OH, A.R.), anhydrous ethanol (C_2H_5OH, A.R.) and RDX were commercially available and used without further purification. Ultrapure H_2O (18.2 MΩ cm) was self-made in the laboratory.

Synthesis of star-like Co-ZIF-L

1.164 g of $Co(NO_3)_2 \cdot 6H_2O$ was dissolved in 10 mL of H_2O to form solution A, and 7.822 g of 2-MI was dissolved in 240 mL of H_2O to form solution B. Under vigorous stirring, solution A was poured into solution B. After 30 min of stirring, the mixture was allowed to stand for 18 h at room temperature. The product was collected by centrifugation and washed with H_2O and C_2H_5OH for several times. Finally, the product was vacuum dried at 50 °C to obtain star-like Co-ZIF-L (SL-Co-ZIF-L) with a pinkish-purple color.

Synthesis of ZIF-67

ZIF-67 with a rhombic dodecahedron morphology was prepared by the method reported in the literature with minor modifications.[1] 0.873 g of $Co(NO_3)_2 \cdot 6H_2O$ was dissolved in 30 mL of CH_3OH to form solution A, and 1.97 g of 2-MI was dissolved in 30 mL of CH_3OH to form solution B. Under vigorous stirring, solution A was poured into solution B. After 10 min of stirring, the mixture was allowed to stand for 24 h at room temperature. The product was collected by centrifugation and washed with CH_3OH for several times. Finally, the product was vacuum dried at 50 °C to obtain ZIF-67 with a pinkish-purple color.

Characterization

Scanning electron microscope (SEM) images were taken using a S-4800 FE-SEM (Hitachi, Japan). Transmission electron microscope (TEM) images were taken using a JEM-2100 TEM (JEOL, Japan). High-angle annular dark-field scanning transmission electron microscopy (HAADF-STEM) and energy-dispersive X-ray spectroscopy

(EDS) were carried out using a JEM-2100F FEG-TEM (JEOL, Japan). Powder X-ray diffraction (PXRD) tests were carried out on a D2-PHASER X-ray diffractometer (Bruker, Germany) using Cu Kα radiation (λ = 1.54184 Å) as the X-ray source, and the scanning speed was 2.4 ° min^{-1}. Fourier transform infrared (FT-IR) spectra were recorded in the range of 4000~400 cm^{-1} on a Tensor-27 infrared spectrometer (Bruker, Germany) using KBr pellets. X-ray photoelectron spectroscopy (XPS) analysis was performed on a K-Alpha XPS spectrometer (Thermo Fisher Scientific, USA). The C 1s line at 284.8 eV was used to calibrate the binding energies. Nitrogen adsorption-desorption isotherm experiments were performed at 77 K on a BELSORP-max II gas sorption instrument (MicrotracBEL, Japan). Thermogravimetric (TG) analyses were performed on a Q600 SDT TGA-DTA-DSC instrument (Thermal Analysis, USA) in N_2 atmosphere with a heating rate of 10 °C min^{-1} from 30 to 600 °C. Differential scanning calorimetry (DSC) analyses were performed on a DSC 204 HP differential scanning calorimeter (Netzsch, Germany). Nitrogen with a flow rate of 50 mL min^{-1} was used as the test atmosphere. During DSC measurements, the catalyst was mixed with RDX at a mass ratio of 1:4 in all situations, and the total mass was around 1.0 mg. TG-DSC-MS-FTIR measurements were carried out on a STA 449F3 TG-DSC simultaneous thermal analyzer (Netzsch, Germany) combined with an infrared spectrometer and a QMS403C quadropole mass spectrometer. The heating rate was 10 °C min^{-1} and argon was used as the carrier gas.

Computational methods

Spin-polarized DFT calculations were performed using the Vienna ab initio simulation package (VASP).[2,3] The generalized gradient approximation proposed by Perdew, Burke, and Ernzerhof (GGA-PBE) is selected for the exchange-correlation potential.[4] The pseudo-potential was described by the projector-augmented-wave (PAW) method.[5] The geometry optimization is performed until the Hellmann-Feynman force on each atom is smaller than 0.02 eV $Å^{-1}$. The energy criterion is set to 10^{-6} eV in iterative solution of the Kohn-Sham equation. Dimer method is used to find the transition states.[6,7]

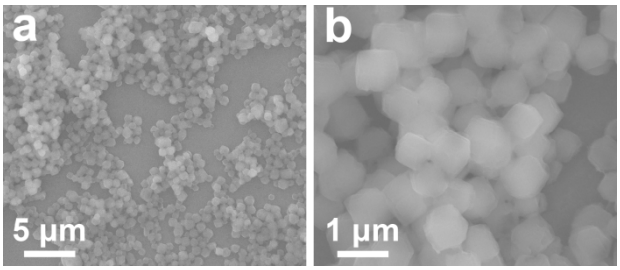

Fig. S1 SEM images of ZIF-67 with a rhombic dodecahedron morphology.

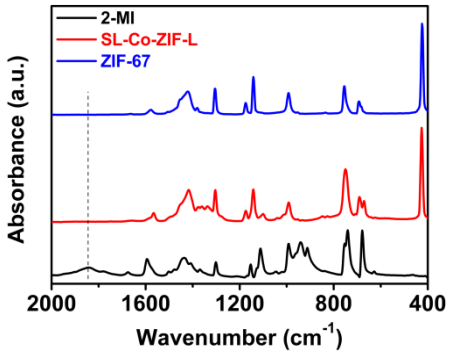

Fig. S2 FT-IR spectra of 2-MI, SL-Co-ZIF-L and ZIF-67.

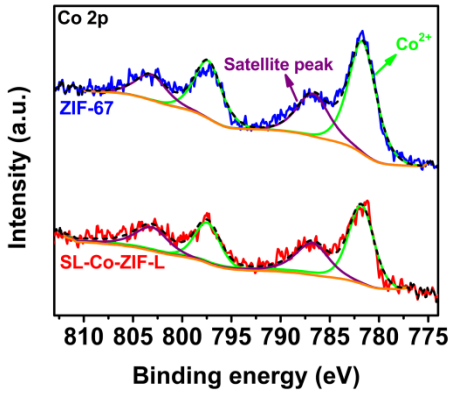

Fig. S3 Co 2p XPS spectra of SL-Co-ZIF-L and ZIF-67.

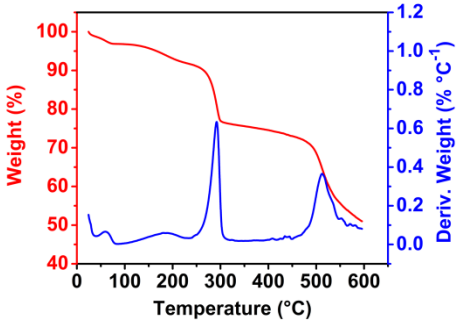

Fig. S4 TG-DTG curves of SL-Co-ZIF-L.

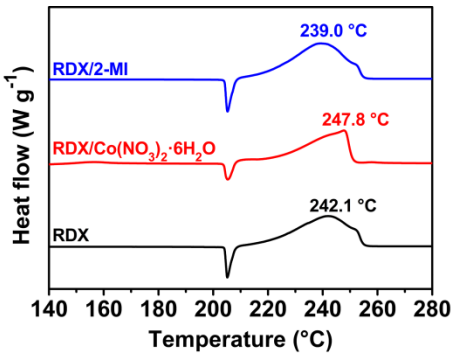

Fig. S5 DSC curves of RDX, RDX/$Co(NO_3)_2 \cdot 6H_2O$ and RDX/2-MI.

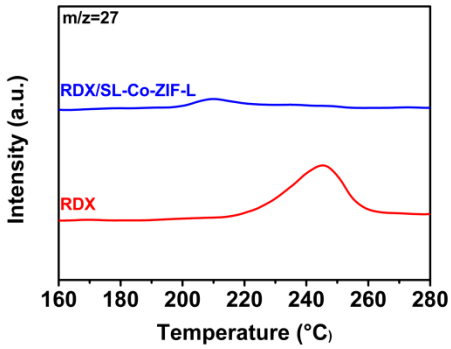

Fig. S6 MS curves (m/z=27) during the thermal decomposition of pure RDX and RDX/SL-Co-ZIF-L.

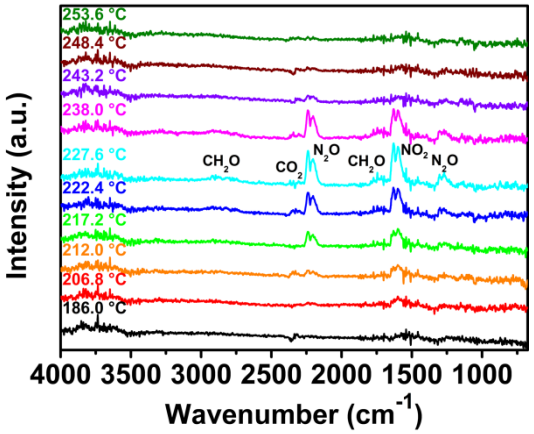

Fig. S7 *in situ* FT-IR spectra of gaseous products during the thermal decomposition of RDX/ZIF-67.

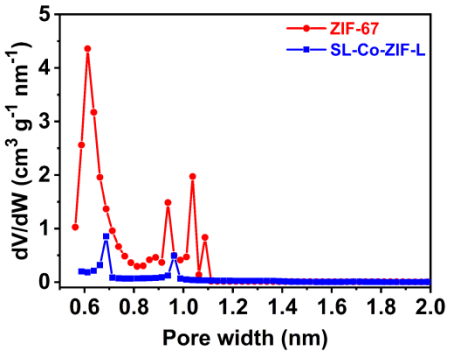

Fig. S8 Micropore size distribution curves of ZIF-67 and SL-Co-ZIF-L.

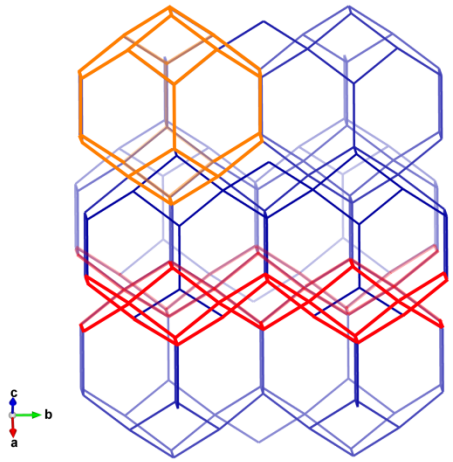

Fig. S9 Relationship between 2D layered Co-ZIF-L and ZIF-67 with a 3D sodalite topology. ZIF-67 framework is blue-colored with a sodalite cage highlighted in orange and 2D layered Co-ZIF-L is red-colored. Only the network of Co atoms is shown.

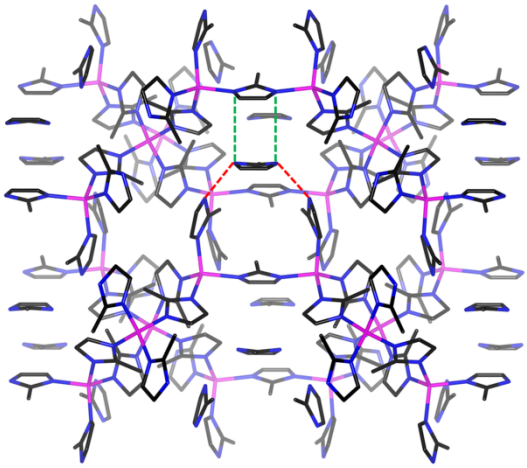

Fig. S10 Two types of interactions (labeled respectively using red and green dotted line) between adjacent 2D layers of Co-ZIF-L. Co: purple; C: black; N: blue. Hydrogen atoms are omitted for clarity.

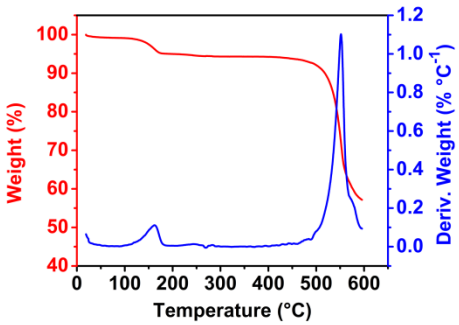

Fig. S11 TG-DTG curves of ZIF-67.

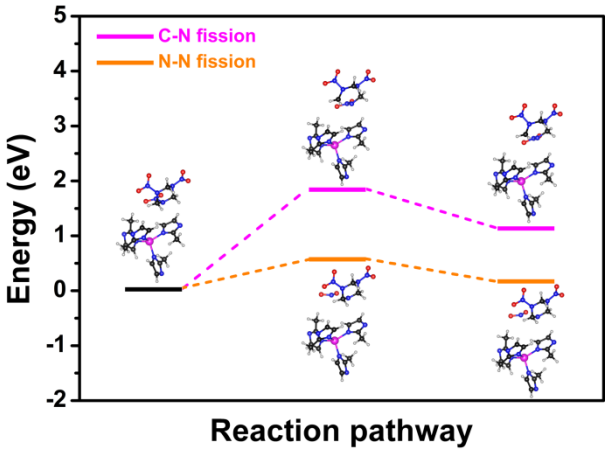

Fig. S12 Free energy for N-N fission and C-N fission decomposition pathway of RDX/ZIF-67.

Table S1 The catalytic performance of SL-Co-ZIF-L and some other existing catalysts towards the thermal decomposition of RDX.

Catalysts	Mass ratio[a]	T_p[b] (°C)	ΔT_p[c] (°C)	ΔH[d] (J g^{-1})	$GR_{\Delta H}$[e] (%)
SL-Co-ZIF-L	1:4	199.2	-42.6	2245	+50.8
ZIF-67	1:4	219.7	-22.4	2381	+59.9
$[PbZn(TATT)(OH)(H_2O)]_n$[8]	1:4	215.5	-24.8	1474	+74.2
$[Co_2(1\text{-mbt})_2(N_3)_4]_n$[9]	1:3	212	-34	/	/
$[Pb(bta)(H_2O)]_n$[10]	1:4	230.1	-10.1	1252	+48.0
$[Ag_2(5\text{-ATZ})(N_3)]$[11]	1:3	228.9	-17.5	/	/
$[Ag_3(H_2ZTO)_3(NO_3)_2(CH_3COO)]_n$[12]	1:4	213.5	-26.7	1128	+33.3
$[Pb(Htztr)_2(H_2O)]_n$[13]	1:3	230	-16	/	/
$[Pb_2(C_5H_3N_5O_5)_2(NMP)\cdot NMP]_n$[14]	1:3	246.2	-2.0	1269.7	-6.8
GO-Cu-DBT[15]	1:4	242.7	-1.6	2242.7	+4.1
GO-T-Co-T[16]	1:4	248.1	+5.4	2248.8	+24.5
$CuFe_2O_4/g\text{-}C_3N_4$[17]	1:4	231.7	-10.6	2325	+58.1
$Bi_2WO_6/g\text{-}C_3N_4$[18]	1:4	235.8	-6.5	/	/
$K_2Pb[Cu(NO_2)_6]$[19]	1:5	238.7	-3.6	1316	-37.2
$CuCo_2O_4$[20]	1:4	236.1	-6.2	/	/
Cu-Co/GO(Ar)[21]	1:4	228.6	-13.7	/	/
$CuFe_2O_4/GO$[22]	1:4	220.34	-20.93	/	/
$MgFe_2O_4$-GO[23]	1:4	234.62	-8.25	/	/
$PbZrO_3/GO$[24]	1:4	217.99	-24.35	/	/
GT-Co[25]	1:4	243.6	+1.3	1886	+4.1
GO enveloped Bi_2WO_6[26]	1:4	208.5	-34.4	1816	+127.9
GO-$MgWO_4$[27]	1:4	213.6	-28.7	/	/

[a] Mass ratio of catalyst to RDX in their compounds. [b] Thermal decomposition peak temperature of RDX/catalyst compounds. [c] Change of thermal decomposition peak temperature of RDX/catalyst compounds compared with pure RDX. [d] Heat release of RDX/catalyst compounds during thermal decomposition process. [e] Growth rate of heat release of RDX/catalyst compounds compared with pure RDX.

Table S2 Thermodecomposition peak temperature of RDX/SL-Co-ZIF-L and pure RDX under different heating rates and corresponding kinetic parameters estimated by Kissinger's and Ozawa's methods.

Samples	Heating rate (°C min^{-1})	T_p (°C)	E_k (kJ mol^{-1})	lnA_k (s^{-1})	R_k	E_o (kJ mol^{-1})	R_o
RDX/SL-Co-ZIF-L	5	192.3	214.28	54.81	0.9838	211.21	0.9848
	10	199.2					
	15	202.0					
	20	203.4					
RDX	5	233.8	191.22	44.54	0.9972	189.97	0.9975
	10	242.1					
	15	246.1					
	20	249.0					

References

1 Z. F. Huang, J. Song, K. Li, M. Tahir, Y. T. Wang, L. Pan, L. Wang, X. Zhang and J. J. Zou, *J. Am. Chem. Soc.*, 2016, **138**, 1359−1365.
2 G. Kresse and J. Furthmüller, *Comp. Mater. Sci.*, 1996, **6**, 15–50.
3 G. Kresse and J. Furthmüller, *Phys. Rev. B*, 1996, **54**, 11169–11186.
4 J. P. Perdew, K. Burke and M. Ernzerhof, *Phy. Rev. Lett.*, 1996, **77**, 3865–3868.
5 P. Blöchl, *Phys. Rev. B*, 1994, **50**, 17953–17979.
6 G. Henkelman and H. Jónsson, *J. Chem. Phys.*, 1999, **111**, 7010–7022.
7 A. Heyden, A. T. Bell and F. J. Keil, *J. Chem. Phys.*, 2005, **123**, 224101.
8 S. Wu, G. Lin, Z. Yang, Q. Yang, Q. Wei, G. Xie, S. Chen, S. Gao and J. Y. Lu, *New J. Chem.*, 2019, **43**, 14336–14342.
9 X. Ma, Y. Liu, W. Song, Z. Wang, X. Liu, G. Xie, S. Chen and S. Gao, *Dalton Trans.*, 2018, **47**, 12092–12104.
10 Q. Yang, X. Song, W. Zhang, L Hou, Q. Gong, G. Xie, Q. Wei, S. Chen and S. Gao, *Dalton Trans.*, 2017, **46**, 2626–2634.
11 X. Qu, Q. Yang, J. Han, Q. Wei, G. Xie, S. Chen and S. Gao, *RSC Adv.*, 2016, **6**, 46212–46217.
12 X. Song, S. Zhang, G. Zhao, W. Zhang, D. Chen, Q. Yang, Q. Wei, G. Xie, D. Yang, S. Chen and S. Gao, *RSC Adv.*, 2016, **6**, 93231–93237.
13 W. Gao, X. Liu, Z. Su, S. Zhang, Q. Yang, Q. Wei, S. Chen, G. Xie, X. Yang and S. Gao, *J. Mater. Chem. A*, 2014, **2**, 11958–11965.
14 J. J. Liu, Z. L. Liu, J. Cheng and D. Fang, *J. Solid State Chem.*, 2013, **200**, 43–48.
15 X. X. Zhang, W. He, S. W. Chen, J. Y. Lyu, Z. Guo, M. Gozin and Q. L. Yan, *Adv. Compos. Hybrid Mater.*, 2019, **2**, 289–300.
16 S. Hanafi, D. Trache, W. He, W. X. Xie, A. Mezroua and Q. L. Yan, *J. Phys. Chem. C*, 2020, **124**, 5182−5195.
17 C. Wan, J. Li, S. Chen, W. Wang and K. Xu, *J. Anal. Appl. Pyrol.*, 2021, **160**, 105372.
18 J. Wang, X. Lian, S. Chen, H. Li and K. Xu, *J. Colloid Interf. Sci.*, 2022, **610**, 842–853.
19 H. Li, B. Liu, Y. Xu, C. Wang, Z. Sun, H. Li, E. Yao, J. Yi, Z. Qin and F. Zhao, *J. Anal. Appl. Pyrol.*, 2021, **157**, 105228.
20 J. Wang, S. Chen, Q. Tang, J. Li and K. Xu, *CrystEngComm*, 2021, **23**, 4522–4533.
21 J. Wang, X. Lian, Q. Yan, D. Gao, F. Zhao and K. Xu, *ACS Appl. Mater. Interfaces*, 2020, **12**, 28496−28509.
22 B. Liu, W. Wang, J. Wang, Y. Zhang, K. Xu and F. Zhao, *J. Nanopart. Res.*, 2019, **21**, 48.
23 W. Wang, B. Liu, K. Xu, Y. Zu, J. Song and F. Zhao, *Ceram. Int.*, 2018, **44**, 19016–19020.

24 B. Liu, Y. Zhang, W. Wang, H. Gao, K. Xu and F. Zhao, *Chin. J. Explos. Prop.*, 2018, **41**, 334–339.
25 W. He, J. H. Guo, C. K. Cao, X. K. Liu, J. Y. Lv, S. W. Chen, P. J. Liu and Q. L. Yan, *J. Phys. Chem. C*, 2018, **122**, 14714−14724.
26 Y. Zhang, L. Xiao, K. Xu, J. Song and F. Zhao, *RSC Adv.*, 2016, **6**, 42428–42434.
27 Y. Zu, Y. Zhang, K. Xu and F. Zhao, *RSC Adv.*, 2016, **6**, 31046–31052.